Research Square

Preprints are preliminary reports that have not undergone peer review.
They should not be considered conclusive, used to inform clinical practice,
or referenced by the media as validated information.

Physicochemical Characterization, Cytotoxicity, and Antimicrobial Activity of Polymeric Nanoparticles for Ocular Delivery of Norfloxacin

İclal ÖZDEMİR
Anadolu University
Kadir AYKAÇ
Erzincan Binali Yıldırım University
Ceyda KÖROĞLU ÖZMEN
Anadolu University
Behiye ŞENEL
Anadolu University
Pervin SOYER
Anadolu University
Ebru BAŞARAN
ebcengiz@anadolu.edu.tr
Anadolu University

Research Article

Keywords: Norfloxacin, Polymeric nanoparticles, Spray drying, Eudragit® RS 100, Polycaprolactone

Posted Date: November 5th, 2026

DOI: https://doi.org/10.21203/rs.3.rs-10984628/v1

License: This work is licensed under a Creative Commons Attribution 4.0 International License.
Read Full License

Additional Declarations: No competing interests reported.

PHYSICOCHEMICAL CHARACTERIZATION, CYTOTOXICITY, AND ANTIMICROBIAL ACTIVITY OF POLYMERIC NANOPARTICLES FOR OCULAR DELIVERY OF NORFLOXACIN

İclal ÖZDEMİR[1], Kadir AYKAÇ[2], Ceyda KÖROĞLU ÖZMEN[3], Behiye ŞENEL[3], Pervin SOYER[4], Ebru BAŞARAN[1]*

[1]Anadolu University, Faculty of Pharmacy, Department of Pharmaceutical Technology, 26470, Eskisehir, TÜRKİYE

[2]Erzincan Binali Yıldırım University, Faculty of Pharmacy, Department of Pharmaceutical Technology, Erzincan, TÜRKİYE

[3]Anadolu University, Faculty of Pharmacy, Department of Pharmaceutical Biotechnology, 26470, Eskisehir, TÜRKİYE

[4]Anadolu University, Faculty of Pharmacy, Department of Pharmaceutical Microbiology 26470, Eskisehir, TÜRKİYE

*Corresponding Author: ebcengiz@anadolu.edu.tr

Abstract

Ocular infections, can lead to severe complications, and may result in vision loss, if not treated effectively. Norfloxacin (NFX), a broad-spectrum fluoroquinolone antibiotic, acts by inhibiting bacterial DNA replication and transcription and is effective against drug-resistant pathogens commonly associated with serious ocular infections. However, its poor water solubility limits its therapeutic potential for ocular delivery. In this study nanoparticles was formulated with Eudragit® RS 100 (ERS100) and Polycaprolactone (PCL) to enhance the ocular bioavailability of NFX. The nanoparticles were prepared using the spray-drying method. According to the characterization studies the optimized formulation exhibited a particle size of 383.43 ± 8.01 nm, a low PDI of 0.135 ± 0.01, and a positively charged zeta potential of +34.97 ± 0.22 mV, indicating excellent stability and favorable interaction with the negatively charged ocular surface, which may enhance the ocular bioavailability of NFX. Cytotoxicity studies using the MTT assay on the human retinal pigment epithelial cell line (ARPE-19) confirmed the ocular safety of the nanoparticles, as their IC_{50} values vastly exceeded their minimum inhibitory concentrations (MICs), indicating a broad therapeutic safety margin. Antimicrobial efficacy was further confirmed through disk diffusion and MIC assays. Based on the obtained results, it can be concluded that ERS100–PCL-based nanoparticles have strong potential as an effective ocular delivery system for NFX in the treatment of severe ocular infections.

Keywords: Norfloxacin, Polymeric nanoparticles, Spray drying, Eudragit® RS 100, Polycaprolactone

Introduction

Ocular infections, which are often of bacterial origin, may arise from various factors, including contact lense use, chronic nasolacrimal duct obstruction, trauma, surgical procedures, aging, and conditions such as dry eye syndrome. If not treated effectively, these infections can lead to serious complications, including vision loss, [1].

Bacterial conjunctivitis, generally characterized by itching, stinging, and tearing of the eye, is considered one of the most prevalent ocular infections worldwide [2,3]. For the treatment of conjunctivitis, broad-spectrum topical antibiotics are commonly initiated based on the assumption of the bacterial etiology [3,4]. Topical administration is generally preferred over systemic antibiotic therapy due to its ease of dosing, suitability for self-administration, and ability to achieve higher drug concentrations at the site of infection, thereby enabling more rapid and sufficient treatment [4,5].

Among the broad spectrum antibiotics used for the treatment of ocular infections, fluoroquinolones such as lomefloxacin, ciprofloxacin, ofloxacin, levofloxacin, and norfloxacin (NFX) are widely used because of their ability to inhibit bacterial DNA replication and RNA synthesis. Furthermore, these agents exhibit potent bactericidal activity against drug-resistant pathogens including, *Staphylococcus aureus (S. aureus)* and *Pseudomonas aeruginosa (P. aeruginosa),* which are among the most clinically significant bacterial pathogens responsible for ocular infections and are frequently associated with severe inflammation and potential vision loss if not promptly treated [6,7].

NFX is a 4-quinolone derivative with broad-spectrum antibacterial activity against both Gram-positive and Gram-negative bacteria, including *S. aureus and P. aeruginosa.* Its mechanism of action involves the inhibition of DNA gyrase (topoisomerase II) and topoisomerase IV, enzymes essential for bacterial DNA replication, transcription, and repair [8,9]. Although NFX is most commonly used for the treatment of genitourinary infections and acute gastroenteritis, several studies have also demonstrated its antimicrobial efficacy against isolates obtained from conjunctivitis and blepharitis cases [10]. Furthermore, previous studies have reported the safety and effectiveness of NFX in the topical treatment of bacterial ocular infections despite its limited ocular

bioavailability, which is mainly attributed to its lipophilic nature and poor aqueous solubility [8,11].

In addition to the solubility-related limitations of active pharmaceutical ingredients, ocular drug delivery remains highly challenging due the unique anatomical and physiological structure of the eye [12]. Tear turnover rapidly eliminates administered formulations from the ocular surface, thereby limiting drug residence time, while the complex structure of the cornea acts as a natural barrier to both hydrophilic and lipophilic drugs, restricting effective treatment of severe ocular disorders [13,14]. To overcome these barriers and enhance both ocular residence time and drug penetration through the corneal layers, various novel drug delivery systems have been developed [15,16]. Among these systems, polymeric nanoparticles have attracted considerable attention for topical ocular applications targeting both anterior and posterior segment diseases [17,18].

In the present study, NFX-loaded polymeric nanoparticles were formulated using Eudragit® RS 100 (ERS100) and polycaprolactone (PCL) with the aim of prolonging precorneal residence time and improving ocular drug disposition, thereby enhancing therapeutic efficacy [19]. The nanoparticles were prepared using the spray-drying method and were comprehensively characterized in terms of their physicochemical properties [19]. The cytotoxicity of the developed nanoparticles was evaluated using the MTT assay. In addition, their antibacterial efficacy was investigated against a panel of clinically relevant bacterial strains, including *Bacillus subtilis (B. subtilis)*, *S. aureus*, *P. aeruginosa*, and *Escherichia coli (E. coli)*, using disk diffusion and minimum inhibitory concentration (MIC) assays.

Experimental

Materials

NFX was purchased from Sigma (Germany). ERS100 was obtained from Röhm Pharma Polymers (Germany), while PCL was purchased from Sigma (Germany). Acetic acid, acetone, acetonitrile, calcium chloride dihydrate, deutero-chloroform, ethanol, methanol, potassium chloride, sodium bicarbonate, sodium chloride were obtained from Merck (Germany). O-phosphoric acid, potassium phosphate monobasic were purchased from Sigma (Germany). Human retinal pigment epithelium cell line (ARPE-19) was provided

from Sabancı University Nanotechnology Research and Application Center (SUNUM). All other chemicals and reagents used in the study were of analytical grade.

Methods

Preparation of Nanoparticles

The nanoparticles were prepared using the spray-drying method [19]. Briefly, ERS100 (1 g) and/or a mixture of ERS100:PCL (3:1, w/w) (1 g) were dissolved in acetone (100 mL). NFX was added to prepared solutions under mild agitation (200 rpm) to facilitate complete dissolution. The clear solutions were then spray-dried using a Nano Spray Dryer (B90, BUCHI Labortechnik AG, Flawil, Switzerland) with an inlet temperature of 60°C±1°C (outlet temperature of 40°C±5°C). The dry powders were collected and stored in tightly sealed, colored vials at room temperature until being analyzed. Placebo nanoparticles were prepared as described above without the addition of active agent. The efficiency of the spray drying process in terms of the active ingredient was evaluated using the drug recovery equation (Eq 1).

$$\text{Drug recovery (\%)} = (T_{NFX} / I_{NFX}) \times 100 \quad \textbf{(Eq. 1)}$$

In Eq. 1 the where T_{NFX} was the total amount of NFX after spray-drying, I_{NFX} was initial amount of NFX.

Characterization of nanoparticles

Morphology

Scanning electron microscopy (SEM; Hitachi, SPC-900-C SEM, China) was used to analyse the shapes and surface properties of the prepared nanoparticles. The analysis was carried out at a room temperature of 25°C ± 2°C with different magnification rates.

Particle size and zeta potential analyses

Particle size, polydispersity index (PDI) and zeta potential analyses were performed using Malvern Nano ZS (Zetasizer Nano Series, Worcestershire, UK). All nanoparticle samples were dispersed in ethanol immediately prior to analysis. All analyses were repeated three times at a temperature of 25 ± 2 °C.

Thermal analyses

The thermal analyses of the polymeric nanoparticle formulations were performed using a differential scanning calorimetry (DSC; DSC60 Shimadzu, Tokyo, Japan). Samples were

analyzed against an empty aluminum cell as a reference within the temperature range of 30–300°C (10 °C.min^{-1}), under nitrogen gas with a flow rate of 50 mL.min^{-1}. Thermograms of the pure materials were also analyzed and used as references to evaluate the thermal behaviours of the nanoparticles.

Nuclear magnetic resonance analyses

The structural characteristics of the nanoparticles were analyzed by proton nuclear magnetic resonance (^{1}H-NMR) spectroscopy using the Ultra-Shield™ CPMAS NMR spectrometer (Bruker, Rheinstetten, Germany). Deutero-chloroform ($CDCI_3$) was used as the solvent. Spectra of pure polymers and pure NFX were used as references to evaluate the structural differentiaitions during the formulation stages of the nanoparticles.

Fourier transform infrared spectrophotometry analyses

Fourier transform infrared spectroscopy (FT-IR) were recorded in the range of 400–4000 cm^{-1} using a Shimadzu IR Prestige-21 instrument (Tokyo, Japan), which features a deuterated triglycine sulfate (DTGS) detector modified with L-alanine and a Germanium-coated potassium bromide beam splitter. FT-IR spectra of pure polymers and pure NFX were used as references to evaluate the spectra of nanoparticles.

Analytical method validation for norfloxacin quantification

A modified high-performance liquid chromatography (HPLC) method was used for quantitative analyses of NFX in the samples. Method validation was performed following the ICH Q2(R1) guidelines. Shimadzu 20 A (Tokyo, Japan) with GL Sciences Inc. column (Tokyo, Japan; column diameter: 4.6 mm, column length: 15.0 cm, particle diameter: 5 µm and particle size: 100 Å) was used as the instrument. Acetonitrile: phosphate buffer (16:84, v/v, pH: 3) was used as the mobile phase with a flow rate of 1.0 mL.min^{-1}. 5 µL constant amount of samples was injected via an Automatic Injector (Shimadzu, Tokyo, Japan) and Photodiode Array Detector (Shimadzu, Tokyo, Japan) was used at 278 nm while the temperature of the column was set to 30°C±1°C [20].

Drug loading and encapsulation efficiency

Accurately weighed nanoparticles (5 mg) were dissolved in 10 mL of a 1:1 (v/v) mixture of methanol and 1% acetic acid and HPLC analyses were performed after proper dilutions for the determination of the total NFX content stated as the drug loading (DL). For the

determination of NFX located on the surface of the nanoparticles, accurately weighed nanoparticle samples (5 mg) were dispersed in 10 mL of 1% acetic acid. The prepared samples were vortexed for 2 minutes, filtered through a 0.45 µm membrane filter, and subsequently analyzed by HPLC (n=3). Encapsulation efficiency (EE), which expresses the amount of NFX placed in the particle lattice, was calculated after determining the difference between the total amount of NFX and the amount of NFX adsorbed onto the surface of the nanoparticles. The LC and encapsulation efficiency (EE) were determined using Equations 2 and 3, respectively.

$$DL\ \% = (T_{NFX} / W_{PNP}) \times 100 \quad \textbf{(Eq. 2)}$$

In Eq. 2 the T_{NFX} was the weight of NFX loaded to the polymeric nanocarrier, and the W_{PNP} carrier was the weight of the polymeric nanocarrier.

$$EE\ \% = [(T_{NFX} - S_{NFX}) / T_{NFX}] \times 100 \quad \textbf{(Eq.3)}$$

In Eq. 3 the where T_{NFX} was the total amount of NFX, S_{NFX} was the amount of free NFX, namely those not being encapsulated and located on the surface of the particles.

In vitro Drug Release and Release Kinetics

The release of NFX from polymeric nanoparticles was analyzed by dialysis membrane (D9777-100FT, Sigma-Aldrich) method [21]. Simulated tear fluid (STF) was prepared as the release medium (pH 7.4) [21]. Considering sink conditions certain amounts of pure NFX, and nanoparticle formulations were weighed and placed into dialysis bags, and 1 mL of STF was added to the membrames and were securely sealed at both ends. The dialysis bags were stirred under a constant speed of 150 rpm in 40 mL of release medium maintained at 34°C ±1°C over 48 hours. At predetermined time intervals, 1 mL samples were withdrawn from the release medium, and an equal volume of simulated STF was replenished maintaining sink conditions. The analyses were performed in triplicate for each formulation. DDSolver software program was also utilized to analyze the release kinetics of NFX from polymeric nanoparticles [22].

Evaluation of the cytotoxicity

The cytotoxicity of pure materials and polymeric nanoparticles were evaluated by MTT assay [23] on human retinal pigment epithelium cell line (ARPE-19) as previously

described [24]. Briefly, ARPE-19 cells were maintained in Dulbecco's Modified Eagle Medium (DMEM) supplemented with 10% FBS and 1% penicillin-streptomycin. For the assay, cells were seeded into 96-well plates at a density of 1×10^4 cells and incubated for 24 hours at 37°C in a humidified atmosphere with 5% CO_2. After the initial incubation, the cells were treated with pure NFX, placebo formulations, and NFX-loaded formulations. Solutions of pure NFX were prepared in concentrations ranging from 50 to 500 $\mu g.mL^{-1}$ and the corresponding amounts of NFX in the loaded formulations were calculated to ensure a consistent dose-response analysis. Following 24 and 48 hours of treatment, the medium was aspirated from cells and 20 µL of MTT solution (5 $mg.mL^{-1}$ in PBS) was added to each well. The plates were then incubated for another 3 hours to allow for formazan crystal formation. Subsequently, the MTT solution was carefully removed, and 200 µL of dimethyl sulfoxide (DMSO) was added to dissolve the resulting formazan crystals. The absorbance was measured at 570 nm using a microplate reader (Cytation 5, BioTek, UK), and the resulting values were used to calculate cell viability. Viability was expressed as a percentage relative to the untreated control cells, which were considered to have 100% viability. All experiments were conducted in triplicates. The IC_{50} values for the effect of each group on the cells were also calculated.

Antimicrobial Activity Tests

Standard bacterial strains *B. subtilis* NRRL B478, *S. aureus* ATCC 6538, *P. aeruginosa* ATCC 27853, and *E. coli* ATCC 3521 were used for antimicrobial activity tests. Samples were prepared by dissolving the formulations in 10% DMSO–methanol solution.

Disc Diffusion Method

Fresh cultures of the test microorganisms were suspended achieve turbidity equivalent to the 0.5 McFarland standard (1.5×10^8 $CFU.mL^{-1}$). Within 15 mins of preparation, 100 µL of the suspension was spread evenly over the entire surface of MHA plates using a sterile Drigalski spatula. After allowing the surface to dry for 3–5 minutes, 6 mm paper discs impregnated with stock concentrations (formulations at 3 $mg.mL^{-1}$ and NFX at 1.5 $mg.mL^{-1}$) were placed on the agar surface using sterile forceps [25]. The plates were inverted and incubated at 37°C for 16–18 hours. After incubation, the diameter of each inhibition zone, excluding the disc, was measured in millimeters (mm) [26].

Determination of minimum inhibitory concentration

The minimum inhibitory concentrations (MIC) of the formulations were determined using the broth microdilution method in 96-well microplates. Two-fold serial dilutions of the formulations (ranging from 0.75 to 0.0003 $mg.mL^{-1}$) and NFX (from 0.37 to 0.0001 $mg.mL^{-1}$) were prepared in cation-adjusted MHB for bacterial strains. Fresh bacterial cultures were adjusted to the 0.5 McFarland standard (approximately 1.5×10^8 $CFU.mL^{-1}$) and diluted in cation-adjusted MHB to yield a final inoculum of $2.5–5 \times 10^5$ $CFU.mL^{-1}$ in each test well. Equal volumes (100 µL) of the formulations and inoculum were dispensed into each well. The test included medium only (sterility control), inoculum only (growth control), and NFX (positive control) [27]. The plates were incubated at 37 °C for 18–20 hours. After incubation, 20 µL of 0.01% resazurin dye was added to each well, followed by an additional 3-hour incubation at 37 °C. The appearance of a pink color indicated microbial growth, whereas a blue-violet color indicated inhibition. MIC values were determined based on these color changes.

Statistical Analysis

All experiments were performed in triplicate, and the results are expressed as mean ± standard deviation (SD). Statistical analyses were performed using GraphPad Prism software (GraphPad Software, San Diego, CA, USA). Differences among the formulation groups were evaluated using one-way analysis of variance (ANOVA), followed by Tukey's multiple-comparison test. A p value < 0.05 was considered statistically significant.

Results and Discussion

Preparation of nanoparticles

In the preliminary studies, various polymers and polymeric mixtures were studied and considering particle size and zeta potential values ERS100 and PCL polymers were selected for further studies. Compositions of the formulations prepared were presented in Table 1.

Table 1. Compositions of the prepared nanoparticle formulations

Code	NFX (mg)	ERS100 (g)	ERS100:PCL (3:1; w/w) (g)	Acetone (mL)
NE0	-	1	-	100
NE1	50	1	-	100
NE2	100	1	-	100
NE3	150	1	-	100
NEP0	-	-	1	100
NEP1	50	-	1	100
NEP2	100	-	1	100
NEP3	150	-	1	100

*ERS100: Eudragit® RS 100, PCL: Polycaprolactone

Characterization of Nanoparticles

Morphology

The morphological analyses of the particles were evaluated with SEM micro-images in our study (Figure 1). The particle sizes and shapes of particulate drug delivery systems formulations are very critical for ocular administration, as they may influence the eye irritation potential of the formulations [28]. SEM micro-images have demonstrated that the nanoparticles were formed with a spherical morphology with considerable smooth surfaces as expected which is preferential for ocular applications (Figure 1).

Particle size and zeta potential analyses

The particle size is a critical factor influencing key parameters including encapsulation efficiency, the release profile of the active substance, mucoadhesive properties and also the stability of particulate drug delivery systems [29]. Moreover, smaller particles are more readily absorbed by precorneal ocular tissues, whereas larger particles exhibit enhanced adhesion to the ocular surface and provide a more sustained drug release profile [21]. The particle size, PDI and zeta potential values of the nanoparticle formulations were presented in Table 2.

The particle sizes of the prepared nanoparticles were relatively comparable (Table 2). Among them, the NE3 formulation exhibited the smallest particle size with 233.47 ± 16.93 nm (Table 2). Increasing the active substance concentration or incorporating PCL into the formulation did not result in a significant change in particle size (Table 2).

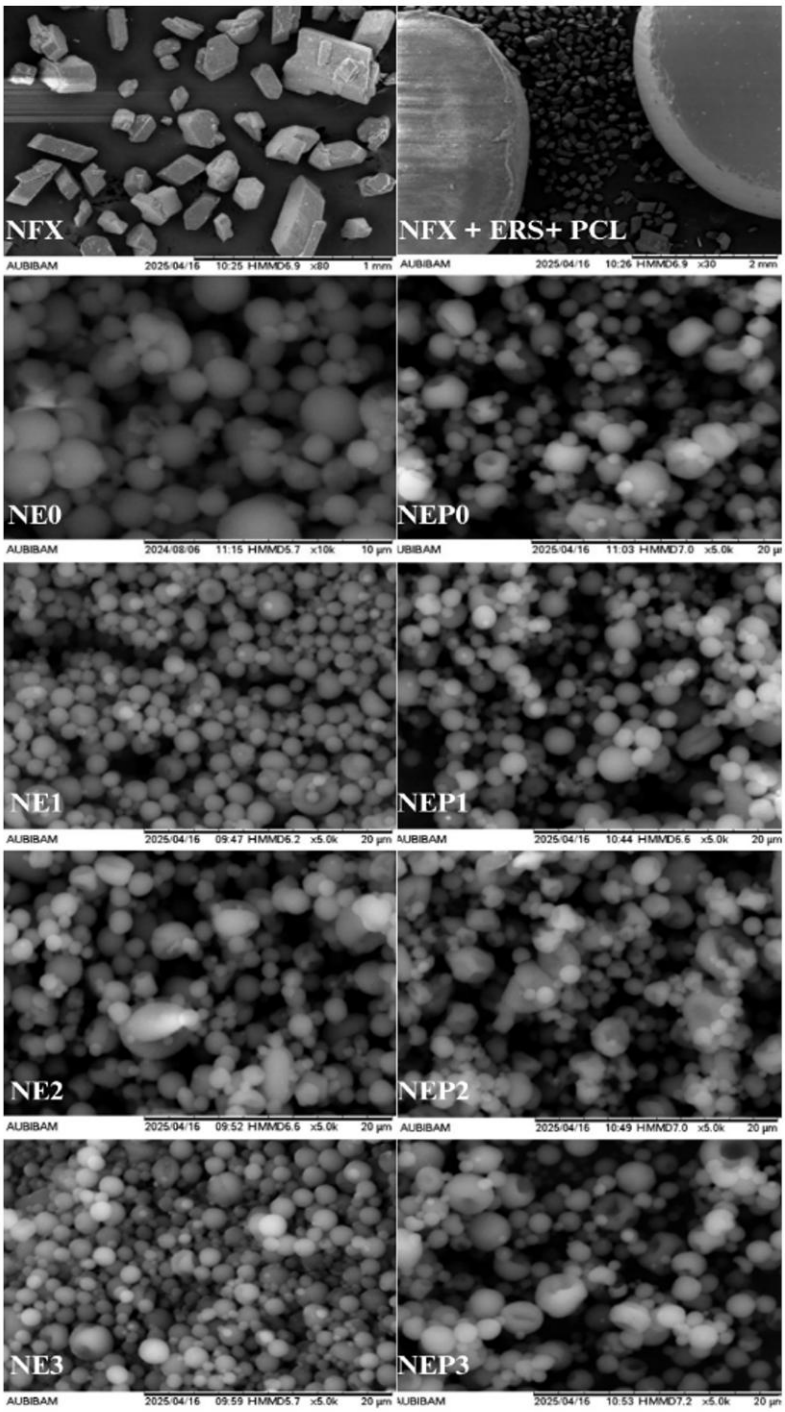


Figure 1. SEM micro-images of NFX, physical mixtures and nanoparticle formulation

Table 2. Particle size, polydispersity index, zeta potential, encapsulation efficiency, drug loading, and drug recovery values of the nanoparticle formulations (Mean ± SE, n = 3).

Code	PS (nm)	PDI	ZP (mV)	EE (%)	DL (%)	Drug recovery (%)
NE0	502.80 ± 8.91	0.452 ± 0.020	+9.63 ± 0.34	-	-	-
NE1	328.73 ± 24.01	0.258 ± 0.070	+14.45 ± 1.38	64.79 ± 0.04	3.20 ± 0.09	67.09 ± 0.01
NE2	235.27 ± 23.51	0.167 ± 0.020	+9.96 ± 2.72	27.72 ± 0.05	6.41 ± 0.16	70.52 ± 0.04
NE3	233.47 ± 16.93	0.214 ± 0.000	+11.85 ± 1.99	24.52 ± 0.09	9.38 ± 0.33	71.89 ± 0.19
NEP0	438.63 ± 22.53	0.381 ± 0.040	+36.20 ± 1.13	-	-	-
NEP1	315.50 ± 13.59	0.272 ± 0.050	+38.43 ± 2.76	65.09 ± 0.01	3.81 ± 0.04	79.95 ± 0.00
NEP2	335.47 ± 4.86	0.161 ± 0.040	+36.30 ± 1.96	43.17 ± 0.12	7.31 ± 0.06	80.39 ± 0.00
NEP3	383.43 ± 8.01	0.135 ± 0.010	+34.97 ± 0.22	32.44 ± 0.08	11.32 ± 0.19	86.78 ± 0.06

PS: Mean particle size, PDI: Polydispersity index, ZP: Zeta potential, EE: Encapsulation efficiency, DL: Drug loading

Notably, placebo nanoparticles were larger in size compared to those loaded with the active substance. This difference may be attributed to physicochemical interactions between NFX and the polymers used in the formulation. The PDI values of the particles, particularly those of the charged formulations, were well below 0.5, indicating a relatively homogeneous particle size distribution [30,31].

Permeability is a significant characteristic of nanoparticles. Particle size and surface charge directly affect intraocular penetration [32]. Studies have shown that membrane permeability decreases as particle size increases, with particles smaller than 400 nm exhibiting greater penetration through polarized epithelial cells [33].

For ocular applications, particle sizes need to be smaller than 10 μm to minimize ocular irritation and discomfort [34,35]. In this regard, the prepared NE and NEP nanoparticles exhibited particle sizes within the desired range, ensuring safe ocular delivery and effective permeation (Table 2).

Zeta potential, which represents the electrical potential at the slipping plane between a particle's surface and the surrounding dispersion medium, is a critical indicator of the colloidal stability of nanoparticle systems. It also correlates with important characteristics like cellular uptake, toxicity, and dissolution behaviors of the particles [36,37]. For a formulation to be considered as physically stable, the zeta potential values should be greater than ± 30 mV [38].

The surfaces of the cornea and conjunctiva are negatively charged due to the sialic acid residues therefore when the ophthalmic formulations have cationic charges, extended adhesion to the anterior segment of the eye will be achieved which will result in enhanced

ocular retention and bioavailability with topical applications [39]. Our analyses results revealed that the zeta potential values of the NE particles were detected to be approximately +10 mV while NEP particles exhibited zeta potential values exceeding +30 mV indicating greater stability potential probably as a result of the orientation of the quaternary ammonium groups of the ERS100 towards the surface of the particles (Table 2). Since the formulations will be applied topically, the prepared nanoparticles are expected to adhere effectively to the anterior segment of the eye and provide efficient treatment due to their cationic zeta potential which is attributed to the positively charged quaternary ammonium groups of ERS100 [40].

Thermal analyses

DSC was performed to evaluate the thermal behavior of polymers and nanoparticles in response to temperature changes and to characterize their structural changes [41,42]. The endothermic melting peak of NFX was observed at 218.79 °C (Figure 2). The DSC thermograms of the semi-crystalline structure of PCL and the amorphous structure of ERS100 were used as a reference to evaluate the thermograms of the nanoparticles (Figure 2). An endothermic peak corresponding to NFX was not detected in the DSC thermogram of the nanoparticle samples indicating that NFX is molecularly dispersed within the polymer matrix and that the amorphous structure of the polymer remains unchanged upon drug loading (Figure 2) [34]. The resulting amorphous structure is expected to enhance the aqueous solubility of the formulation while maintaining sustained drug release [43].

Nuclear magnetic resonance analyses

^{1}H-NMR analyses were employed to investigate the structural characteristics of both the nanoparticles and NFX [40]. In the ^{1}H-NMR spectrum of NFX, the signal observed between 7.54 and 8.64 ppm corresponds to the aromatic protons of NFX, while the peaks at 1.18 ppm and 1.31 ppm are attributed to the CH_3 and CH_2 groups, respectively (Figure 3) [44]. Upon comparison of the NFX-loaded nanoparticle formulations no significant differences were observed among the proposed signals (Figure 3).

The signal in the 8–9 ppm range, characteristic of pure NFX, was also detected in the spectra of the drug-loaded nanoparticles, with reduced intensity (marked with arrows) considering incorporated amount of NFX (Figure 3) suggesting that the active substance

was successfully incorporated into the nanoparticles without significant alteration of its chemical structure [40]. Potential interactions between the formulation components and the active substance were investigated using FT-IR spectroscopy in the wavelength range of 4000–400 cm^{-1} [45].

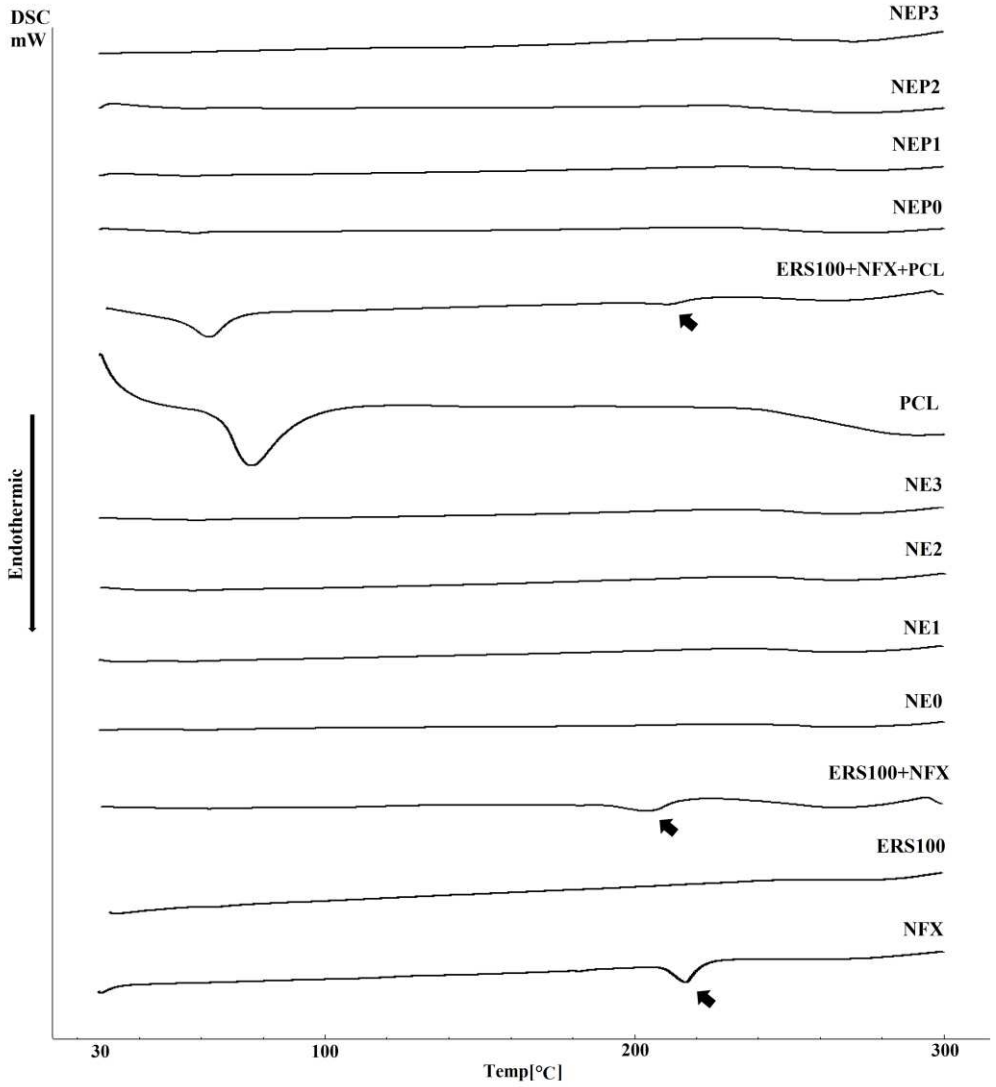


Figure 2. DSC thermograms of pure materials, physical mixtures and nanoparticle formulations (Endothermic melting peaks of NFX was marked with arrows).

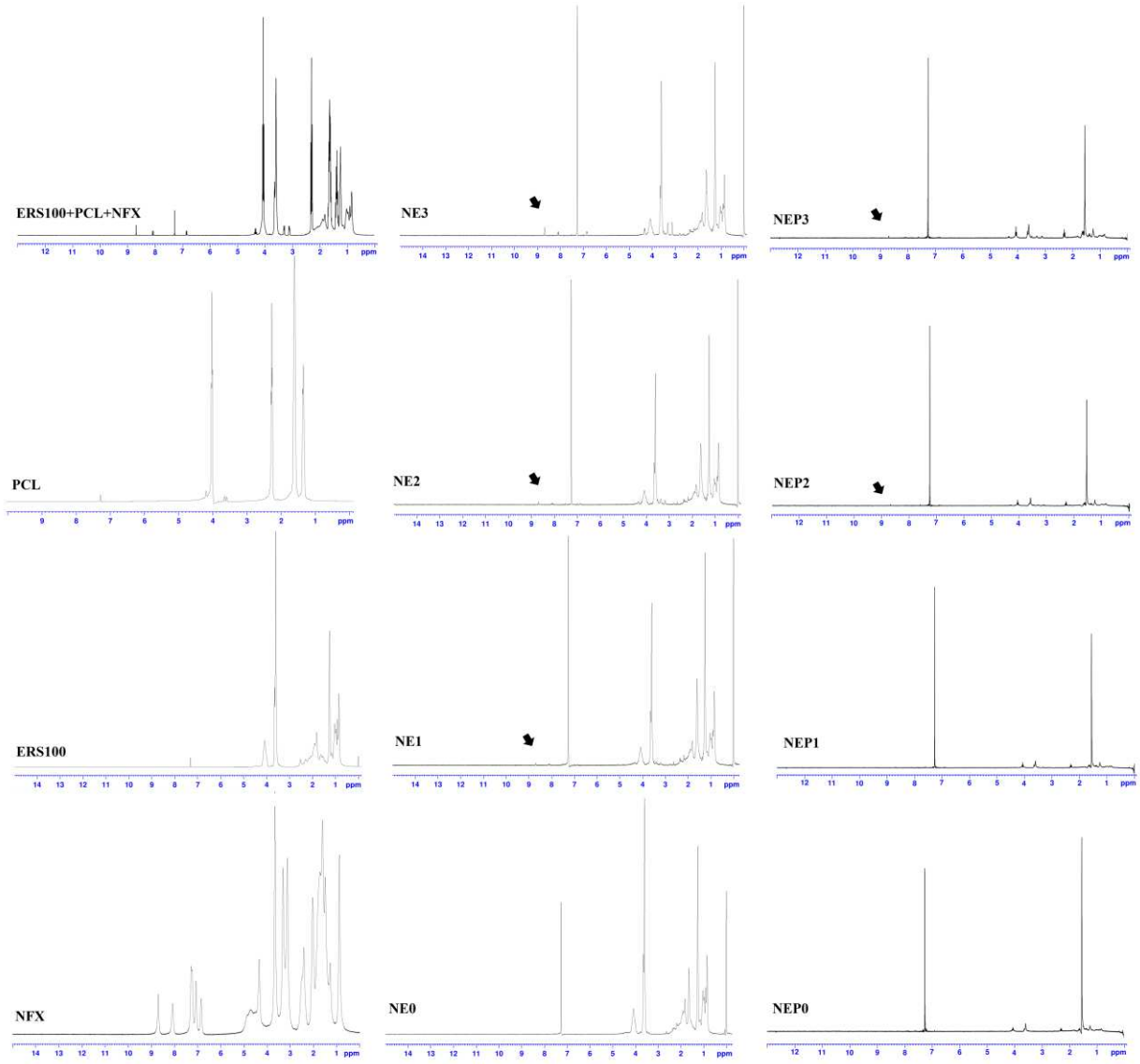


Figure 3. ^{1}H-NMR spectra of pure materials, physical mixtures and nanoparticle formulations

Fourier transform infrared spectrophotometry analyses

A distinct characteristic peak was observed in the FT-IR spectrum of NFX within the range of 3550–3500 cm^{-1}, corresponding to the O–H stretching vibration and indicative of intermolecular hydrogen bonding. The broad absorption band observed between 3500–3300 cm^{-1} is attributed to N–H stretching vibrations in the imino region of the piperazinyl groups. Additionally, the peak observed in the range of 2750–2700 cm^{-1} is associated with the ethyl group, while the band around 2500 cm^{-1} corresponds to the O–H stretching of the carboxylic acid group (Figure 4) [45]. For ERS, a characteristic C–O stretching

peak was observed at 1720 cm^{-1} (Figure 4) [46]. In the FT-IR spectrum of PCL, peaks corresponding to aliphatic C–H stretching vibrations were detected at 2865 and 2942 cm^{-1}. The absorption peak associated with the carbonyl (C=O) stretching appeared at 1721 cm^{-1}, while C–O and C–C stretching vibrations were identified at 1292.9 cm^{-1}. Additionally, characteristic peaks corresponding to C–O–C stretching were observed at 1162 and 1238 cm^{-1} (Figure 4) [47].

The FT-IR spectra of the physical mixtures of NFX and the polymers showed preservation of characteristic peaks, suggesting the absence of chemical interactions during formulation stages. The FT-IR spectra of the nanoparticle formulations exhibited similar profiles, with a noticeable decrease in the intensity of the characteristic peaks of NFX suggesting the successfull incorporation of NFX into the polymer matrix (Figure 4).

Analytical method validation for norfloxacin quantification

The HPLC method was modified and validation studies were performed for the determination of NFX [20]. Analyses results demonstrated a high level of linearity for 1% acetic acid (v/v), with a correlation coefficient (r^2) of 0.9995 and a calibration curve described by the equation $y = 39401x - 30475$. Furthermore, the method met the ICH criteria for accuracy, repeatability, and reproducibility, as accuracy was within the range of 98.0%–102.0%, and RSD values in precision studies were below 2% [48].

Drug loading and Encapsulation Efficiency

The amount of NFX encapsulated in the polymeric matrix of the nanoparticles were presented in Table 2. DL% and EE% were calculated using Equation 1 and Equation 2, respectively. According to the analyses results, formulations NE1 and NEP1 exhibited the highest encapsulation efficiencies, with values of $64.79 \pm 0.04\%$ and $65.09 \pm 0.01\%$, respectively. In contrast, for NE2, NE3, NEP2, and NEP3 formulations, a substantial portion of the active compound was adsorbed onto the particle surfaces. Consequently, as the initial drug concentration increased, a decrease in EE was observed.

This could potentially be attributed to electrostatic attractions within the active agent and the polymers [49]. The incorporation of PCL into the formulation positively influenced both the EE of the active substance and the overall DL. Furthermore, this addition increased drug recovery (Table 2).

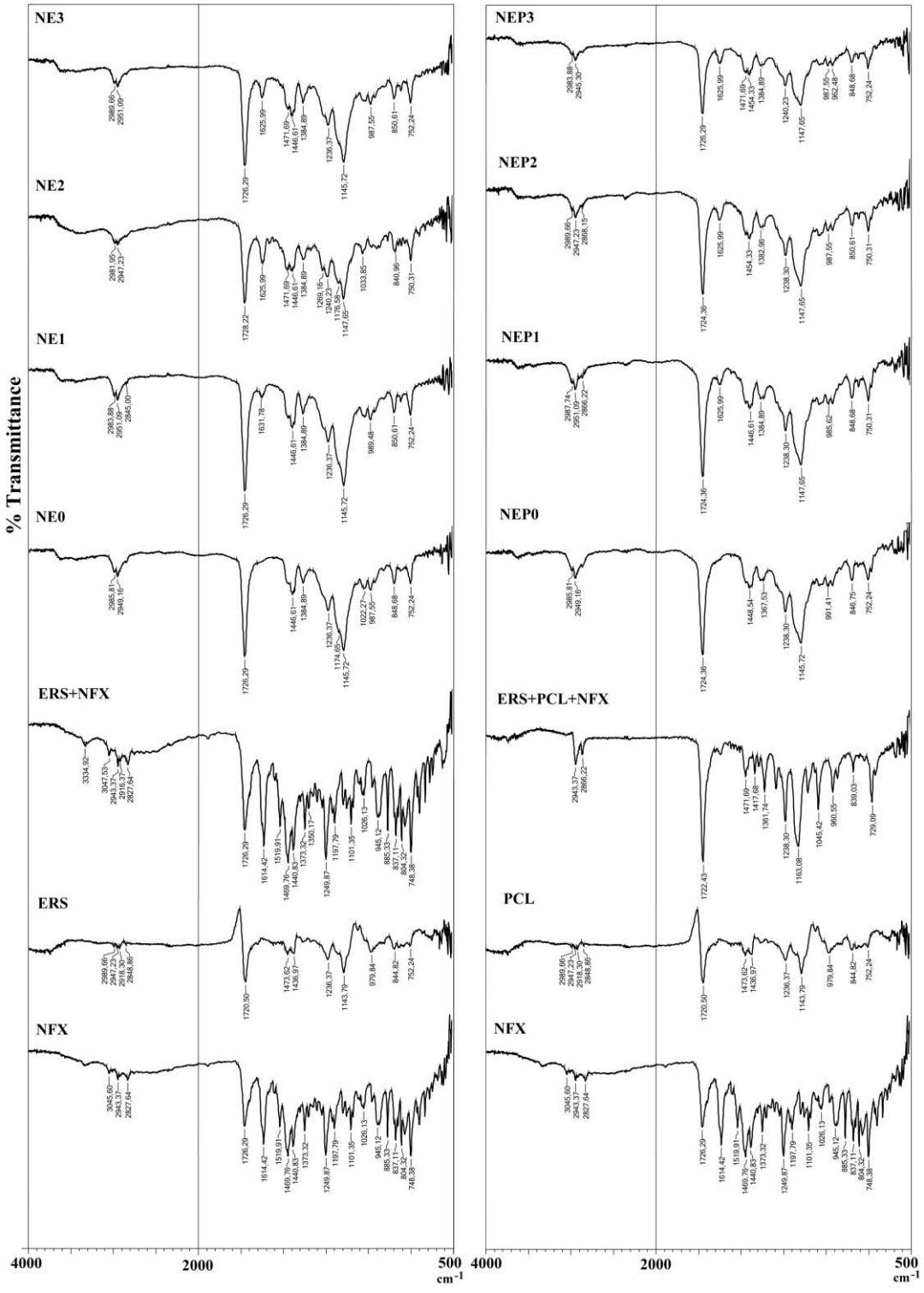


Figure 4. FT-IR spectra of pure materials, physical mixtures and nanoparticle formulations

In vitro Drug Release and Release Kinetics

The *in vitro* release study demonstrated that approximately 60–70% of NFX was released from all nanoparticle formulations within the first 3 to 4 hours. This rapid initial release

is likely attributable to the active substance being primarily adsorbed onto the surface of the polymer matrix [50]. Nevertheless, such an initial burst release could be advantageous for rapidly achieving the minimum effective drug concentration required for antibacterial activity [28]. As presented in Figure 5, NFX release from the nanoparticle formulations extended up to approximately 48 hours.

During the first 30 minutes, the release rate from NEP nanoparticles was higher than that of NE nanoparticles. However, in the subsequent hours, the release profiles of both formulations became comparable and followed a similar pattern. Among these, NE3 exhibited a relatively slower release profile compared to the other formulations. When the release profile of pure NFX was examined, it reached 99% cumulative release within 8 hours, whereas the NE and NEP nanoparticle formulations achieved 99% release at 48 hours (Figure 5). As expected, the use of ERS100 and PCL polymers successfully enabled a sustained and prolonged release of the drug in all nanoparticle formulations. *In vitro* release studies suggest that the ocular application of NFX, a drug with very low water solubility, has the potential to enhance its bioavailability.

To gain insights into the potential *in vivo* release behavior of the prepared nanoparticle formulations, their conformity to various *in vitro* mathematical release models was assessed using the DD-Solver program [22].

To determine the best-fitting kinetic model for the release data, three statistical parameters were evaluated: The adjusted coefficient of determination (R^2_{adj}), Model Selection Criterion (MSC), and Akaike Information Criterion (AIC). The optimal model was identified by a R^2_{adj} value closest to 1, along with the highest MSC and lowest AIC [51]. The results of this evaluation are presented in Table 3.

The release kinetics of pure NFX and the NE1 formulation were found to follow first-order kinetics, indicating that the drug release rate is concentration-dependent [52].

In contrast, the release profiles of all other nanoparticle formulations were best described by the Korsmeyer–Peppas model. This model is commonly employed to analyze drug release from polymeric carrier systems when the exact mechanism is unknown or when the release involves multiple processes such as the diffusion of water into the matrix, swelling of the matrix and dissolution of the matrix [53]. The permeation of the active compound through the membranes is primarily explained by passive diffusion, which is the spontaneous mass transfer of a substance from an area of high concentration to an

area of lower concentration. This diffusion adheres to Fick's Law [54]. In the Korsmeyer-Peppas model, the obtained "n" value is an indicator of Fickian diffusion when n<0.45 the diffusion process is considered to be Fickian [55]. According to Table 3, the "n" value for all nanoparticle formulations is less than 0.45. Thus, it can be concluded that diffusion in the prepared nanoparticle formulations occurs in accordance with Fick's Law [55].

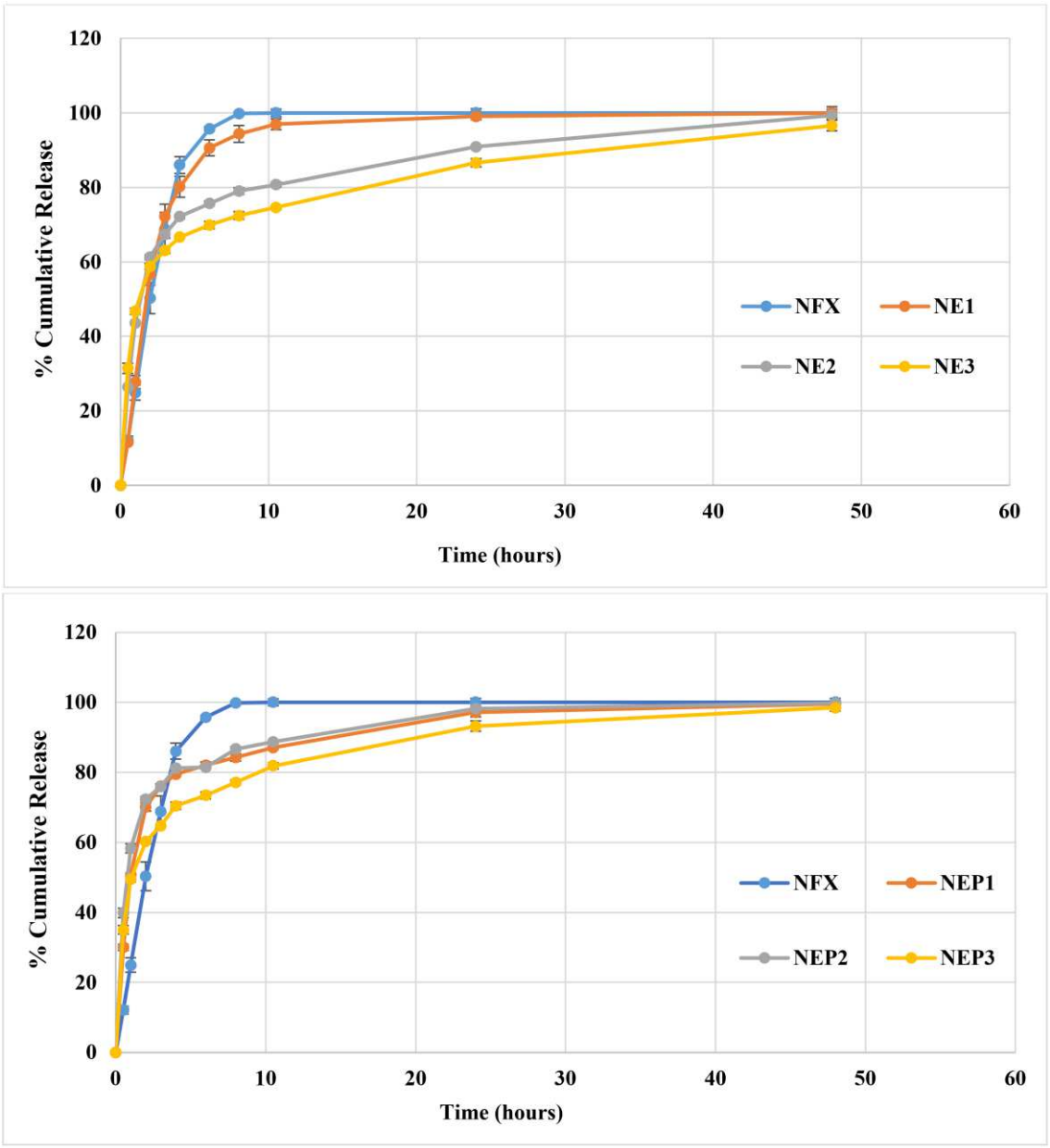


Figure 5. ***In vitro*** **release profiles of NFX and nanoparticle formulations (Mean ± SE, n= 3)**

Evaluation of the Cytotoxicity

The safety profile of drug delivery systems require comprehensive cytotoxicity assessment of their constituent polymeric carriers.

In our study nanoparticles were formulated with ERS, a cationic polymer known for its controlled release and mucoadhesive properties [56] and a blend of PCL which is a biocompatible and biodegradable polymer with ERS100 [57]. Within the scope of this study, the *in vitro* toxicity profiles of placebo nanoparticles, the active substance NFX, and active substance-loaded nanoparticles on ocular cells were evaluated using the MTT cytotoxicity assay. The ARPE-19 was utilized for the MTT cytotoxicity assay, as it is a widely recognized cell model in ocular drug safety studies [58,59]. Although corneal cell lines are traditionally preferred, recent comparative studies have revealed that IC_{50} values obtained from ARPE-19 cells exhibit a stronger correlation with *in vivo* ocular irritation (Draize test scores) compared to those obtained from rabbit corneal cells [60]. Therefore, the MTT assay performed on ARPE-19 cells provides predictive insights for assessing the ocular safety and evaluating the irritation potential of the prepared nanoparticles [58,61].

Cytotoxicity values of all formulations with respect to time and concentration were presented in Figure 6.

According to the MTT analyses results, both the NE0 and the NEP0 formulations were determined to be generally highly biocompatible, as the IC_{50} value could not be determined even at the highest concentrations tested. However, the 24-hour viability values at the 500 $\mu g.mL^{-1}$ concentration, NE0 exhibited lower cytotoxicity compared to NEP0 formulation with 85.19% and 78.11% cytotoxicity values while the difference diminished at the end of 48-hours incubation, with 76.36% and 75.45% viability values respectively (Figure 6).

Our data was supperted by former studies showing the non-toxic, stable, non-dose-dependent cytotoxicity of PCL nanoparticles [62–64]. Similarly, non-toxic characters of the nanoparticles have also been reported for ERS100 formulations [30]. As a result, our findings are compatible with the literature. Although the general principle in the literature suggests that the addition of PCL should mitigate the cationic toxicity potential originating from ERS100 thus enhance biocompatibility [65,66].

Table 3. ***In vitro*** **release kinetic models of NFX and nanoparticle formulations**

Code	Criteria	Zero order	First order	Higuchi	Hixon-Crowell	Hopfenberg	Korsmeyer-Peppas
	k	3.2674	0.3645	22.2922	0.0231	0.0808	43.0771
	R^2_{adj}	-1.0991	**0.9921**	0.3457	-0.1093	0.9863	0.7899
NE1	**AIC**	114.9692	**53.4970**	102.1464	107.9533	60.4757	81.5348
	MSC	-1.3094	**4.2790**	-0.1437	-0.6716	3.6446	0.8955
	n						0.2727
	k	3.0621	0.1670	20.6961	0.0313	0.0313	47.9785
	R^2_{adj}	-1.7248	0.5600	0.1975	0.0137	-0.0724	**0.9329**
NE2	**AIC**	112.7082	92.6517	99.2622	101.5303	103.2920	**64.6265**
	MSC	-1.8103	0.0130	-0.5879	-0.7941	-0.9543	**1.7336**
	n						0.2164
	k	2.9271	0.1213	19.6844	0.0267	0.0267	44.5963
	R^2_{adj}	-1.9152	0.2083	0.1429	-0.2325	-0.3663	**0.9570**
NE3	**AIC**	111.3995	97.0610	97.9335	101.9300	103.9042	**57.9028**
	MSC	-1.9730	-0.6695	-0.7488	-1.1121	-1.2916	**2.0252**
	n						0.2387
	k	3.1849	0.1919	21.9456	0.0344	0.0344	54.4298
	R^2_{adj}	-2.2071	0.4644	-0.0514	-0.2565	-0.3004	**0.8909**
NEP1	**AIC**	115.2408	95.5543	102.9729	104.9330	106.1523	**70.7596**
	MSC	-2.0661	-0.2764	-0.9508	-1.1290	-1.2399	**1.1844**
	n						0.1713
	k	3.2157	0.2159	22.3090	0.0361	0.0361	55.6413
	R^2_{adj}	-2.7387	0.3885	-0.2807	-0.5731	-0.5454	**0.9499**
NEP2	**AIC**	116.0806	96.1644	104.2963	106.5578	107.2034	**62.2833**
	MSC	-2.0661	-0.5878	-1.3271	-1.5327	-1.5914	**1.7700**
	n						0.2123
	k	3.0575	0.1500	20.6923	0.0303	0.0303	47.4174
	R^2_{adj}	-2.0309	0.3676	0.0977	-0.1591	-0.2715	**0.9749**
NEP3	**AIC**	112.8046	95.5673	99.4763	102.2319	104.0904	**53.8037**
	MSC	-2.0326	-0.4655	-0.8209	-1.0714	-1.2404	**2.5740**
	n						0.2382
	k	3.3250	0.4575	23.0147	0.0289	0.1012	49.5456
	R^2_{adj}	-1.3226	**0.9913**	0.2222	-0.0232	0.9651	0.7939
NFX	**AIC**	116.5601	**55.1520**	104.5262	107.5430	71.2180	82.0146
	MSC	-1.4381	**4.1445**	-0.3441	-0.6184	2.6839	0.8918
	n						0.2497

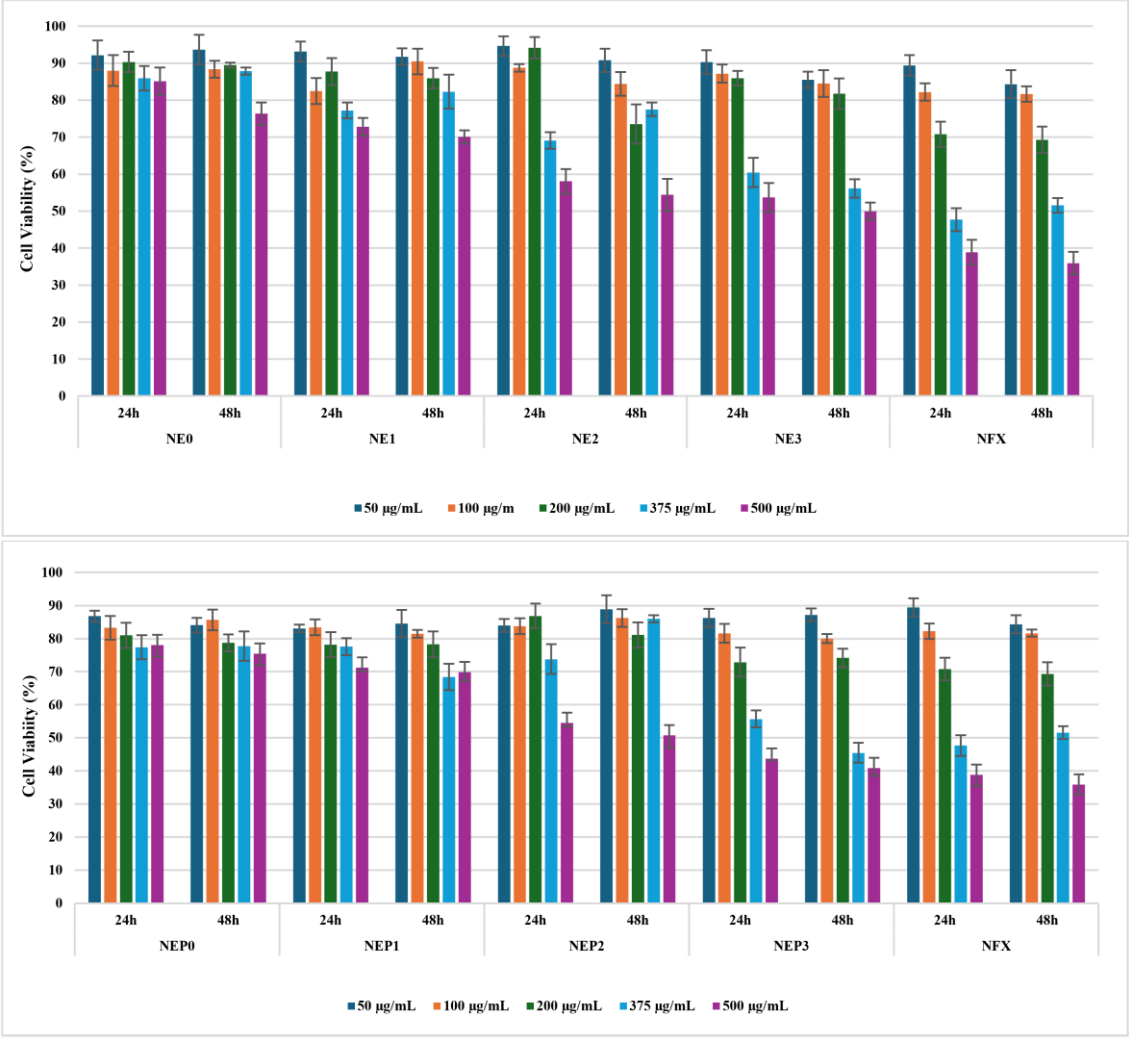


Figure 6. Cytotoxicity results of nanoparticle formulations (n = 3; mean ± SD).

Zeta potential measurements indicated that the PCL incorporation unexpectedly shifted the charge to a more cationic direction. This unanticipated result suggests that the observed minor increase in NEP0 cytotoxicity may be attributed to the resultant highly positive surface charge. Furthermore, studies have demonstrated that the PCL type used in the formulation (80 kDa) may exhibit higher *in vitro* toxicity compared to other low molecular weighted PCL derivatives [67].

In a related study, the cell viability of Human Corneal Epithelial Cells (HCECs) exposed to NFX was investigated using the MTT assay, which demonstrated that NFX concentrations over 375 $\mu g.mL^{-1}$ exhibited dose- and time-dependent cytotoxicity [68]. In our study, a comparable concentration of 375 $\mu g.mL^{-1}$ resulted in a cell viability of 47.96% at 24 hours, which further decreased to 35.92% at 48 hours (Figure 6). Upon the

evaluation of the NFX-loaded formulations, both the NE and NEP series successfully demonstrated a reduction in the cytotoxicity of free NFX. However, formulations characterized by a higher NFX of DL (NE3 and NEP3) exhibited a more pronounced toxic profile. This observation is attributed to their higher overall NFX content and, consequently, lower polymer protection per unit mass relative to other formulations.

This increase in cytotoxicity is therefore interpreted as a direct consequence of the elevated NFX loading. The IC_{50} value for the pure active compound NFX was determined to be 359.4 $\mu g.mL^{-1}$ and 357.8 $\mu g.mL^{-1}$ at 24 and 48 hours, respectively. Formulations containing ERS100 were observed to increase the IC_{50} value of NFX, with cell viability remaining above 50% even at the highest tested concentration. Specifically, the IC_{50} values of NFX in ERS-PCL formulations were elevated to 443.6 $\mu g.mL^{-1}$ and 366.5 $\mu g.mL^{-1}$ at 24 and 48 hours, respectively (Figure 6).

Antimicrobial Activity Tests

Disc diffusion method

The antimicrobial disc diffusion method, also known as the Kirby–Bauer test, is a standard method used to evaluate bacterial susceptibility to antibiotics. The formulations prepared with NFX exhibited variable inhibition zones depending on the tested concentration and bacterial strain (Table 4, Figure 7). Among the Gram-positive strains, *B. subtilis* showed inhibition zones ranging from 24.1 to 33.9 mm, while *S. aureus* exhibited zones between 16.0 and 30.2 mm. Gram-negative strains demonstrated lower sensitivity: *P. aeruginosa* showed inhibition zones of 12.0–21.7 mm, and *E. coli* displayed zones ranging from 18.1 to 29.8 mm. NFX (positive control) consistently produced larger inhibition zones, measuring 33.9–36.1 mm for *B. subtilis* and *S. aureus*, 30.1 mm for *E. coli*, and 29.9 mm for *P. aeruginosa* (Table 4, Figure 7). The drug-free formulations (NE0 and NEP0) produced either no inhibition or only small and highly variable inhibition zones. The relatively large SD values observed for these blank formulations resulted from inconsistent detection of very small inhibition zones among replicate measurements. Because the inhibition boundaries were close to the disc edge, minor differences among replicates resulted in relatively high variability. In contrast, NFX-containing formulations produced clearly defined inhibition zones with substantially lower variability. Statistical differences in inhibition zone diameters among

the formulations were evaluated using one-way ANOVA followed by Tukey's multiple-comparison test, with statistical significance defined as $p < 0.05$.

Table 4. Zone inhibition diameters (mm) of NFX and nanoparticle formulations

Code	*B. subtilis*	*S. aureus*	*P. aeruginosa*	*E. coli*
NFX	36.1 ± 0.4	33.9 ± 0.1	29.9 ± 0.3	30.1 ± 0.4
NE0	-	-	3.3 ± 3.0	3.6 ± 3.5
NE1	24.1 ± 0.3	16.0 ± 0.2	12.0 ± 0.2	18.1 ± 0.3
NE2	28.0 ± 0.2	21.8 ± 0.6	14.0 ± 0.2	21.9 ± 0.4
NE3	29.8 ± 1.1	28.0 ± 0.2	21.7 ± 0.4	29.8 ± 0.4
NEP0	3.3 ± 3.5	-	-	-
NEP1	26.0 ± 0.2	22.2 ± 0.5	12.0 ± 0.2	20.1 ± 0.3
NEP2	29.6 ± 0.7	28.1 ± 0.3	15.8 ± 0.5	24.2 ± 0.5
NEP3	33.9 ± 0.2	30.2 ± 0.5	20.0 ± 0.2	25.1 ± 0.4

Bacillus subtilis (B. subtilis), Staphylococcus aureus (S. aureus), Pseudomonas aeruginosa (P. aeruginosa), Escherichia coli (E. coli)

In the disc diffusion method, Gram-positive strains (*B. subtilis* and *S. aureus*) generally exhibited greater susceptibility than Gram-negative strains, which is consistent with structural differences in their cell walls. Gram-negative bacteria possess an outer membrane enriched with lipopolysaccharides, which decreases permeability to hydrophobic compounds and antibiotics [69]. Notably, *P. aeruginosa* displayed the lowest susceptibility, consistent with its well-documented multidrug resistance mechanisms, including efflux pumps and low outer membrane permeability [70].

Determination of minimum ınhibitory concentration (MIC)

MIC test is a standard method used to determine the lowest concentration of an antimicrobial agent that visibly inhibits microbial growth. The MIC values of the formulations were determined within the range of 0.04 and 0.75 $\mu g.mL^{-1}$ (Table 5).

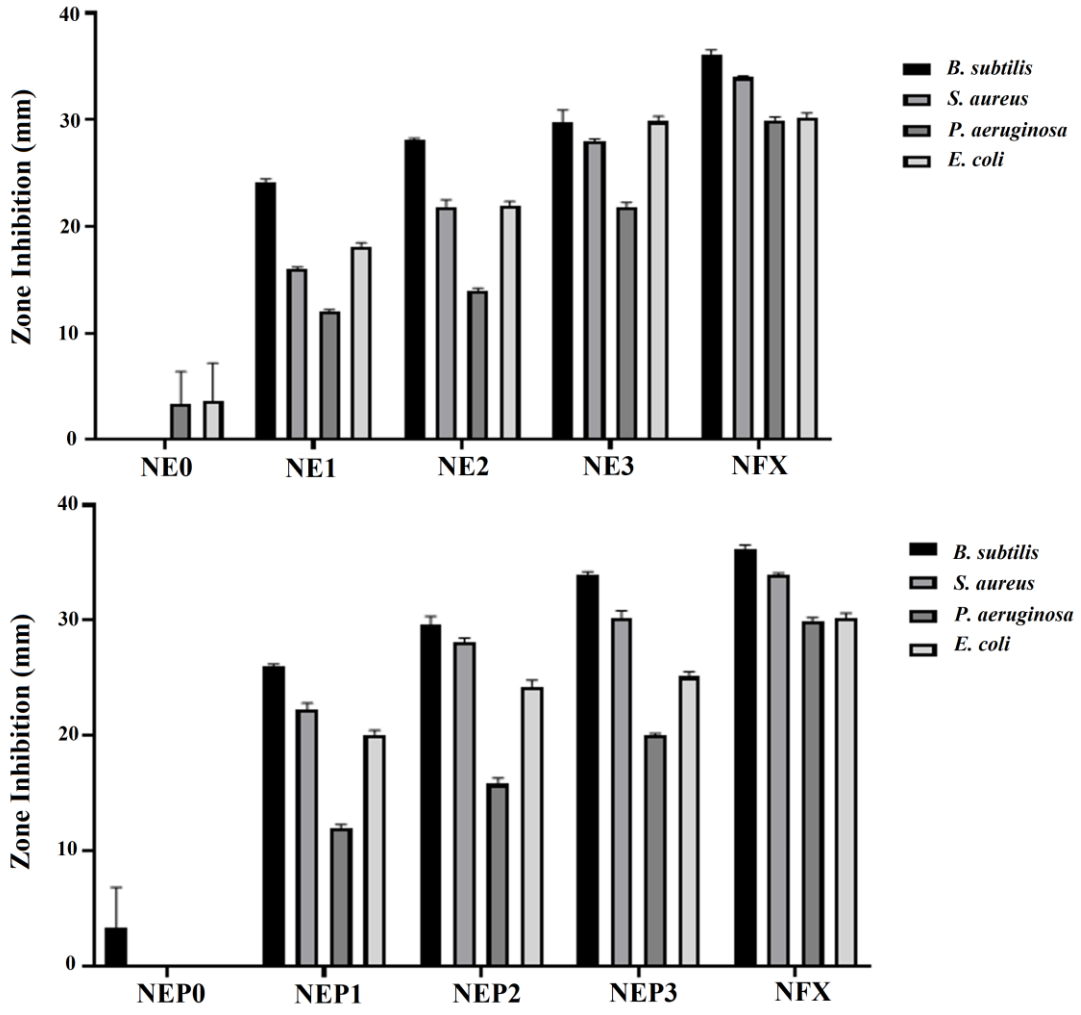


Figure 7. Inhibition zone diameters of NFX and nanoparticle formulations against the tested bacterial strains. Data are presented as mean ± SD (n = 3). Statistical comparisons among formulation groups were performed using one-way ANOVA followed by Tukey's multiple-comparison test. Statistical significance was accepted at $p < 0.05$.

For the NE series, the lowest MIC values were observed against *S. aureus*, *P. aeruginosa*, and *E. coli* (0.04–0.18 μg.mL^{-1}), while slightly higher MIC values were recorded for *B. subtilis* (0.09–0.37 μg.mL^{-1}). In contrast, for the NEP series, identical MIC concentrations (0.04–0.18 μg.mL^{-1}) were observed across all tested microorganisms. NFX, consistent with its well-documented efficacy, exhibited markedly lower MIC values (0.002–0.005 μg.mL^{-1}) against the tested strains. MIC determinations were performed in triplicate, and identical MIC endpoints were obtained across the replicate experiments. Since MIC represents a discrete endpoint derived from two-fold serial dilutions rather than a continuous quantitative measurement, the results are reported as modal MIC values rather than mean ± SD (Table 5).

The results have demonstrated that the NFX-based formulations retained antimicrobial activity against both Gram-positive and Gram-negative bacteria, although their efficacy was reduced compared to the pure NFX standard. This reduction may be attributed to formulation-related factors that influence drug release and bioavailability, such as excipient interactions or altered diffusion through the agar medium [71]. The obtained MIC values revealed a dose-dependent activity, where higher formulation concentrations resulted in increased inhibition. Although the inhibitory concentrations were higher than those of pure NFX, the formulations still exhibited clinically significant antimicrobial activity. The consistency between disc diffusion and MIC results further validates the antimicrobial potential of these formulations.

Table 5. MIC values of NFX and nanoparticle formulations (μg.mL^{-1})

Code	*B. subtilis*	*S. aureus*	*P. aeruginosa*	*E. coli*
NFX	0.005	0.005	0.005	0.002
NE0	-	-	≥0.75	≥0.75
NE1	0.37	0.18	0.18	0.18
NE2	0.18	0.09	0.09	0.09
NE3	0.09	0.04	0.04	0.04
NEP0	≥0.75	-	≥0.75	≥0.75
NEP1	0.18	0.18	0.18	0.18
NEP2	0.09	0.09	0.09	0.09
NEP3	0.04	0.04	0.04	0.04

Bacillus subtilis (B. subtilis), Staphylococcus aureus (S. aureus), Pseudomonas aeruginosa (P. aeruginosa), Escherichia coli (E. coli)

Furthermore, evaluating the clinical relevance of these findings alongside the *in vitro* release profiles clearly demonstrates that the formulations provide an immediately effective drug dose. Notably, even with the NE1 and NEP1 formulations (which contain the lowest NFX content) concentrations of NFX approximately 2 and 7 μg.mL^{-1} were achieved at the earliest sampling time point (30 minutes), respectively (NFX MIC range: 0.002–0.005 μg.mL^{-1}). This confirms that the prepared nanoparticles possess the capacity to achieve and maintain local drug concentrations well above the inhibitory threshold from the moment of initial administration.

Conclusion

The anatomical and physiological barriers of the eye, combined with the low solubility of the active substance, result in limited bioavailability of topically administered drugs in the treatment of severe ocular infections. Therefore, alternative strategies are required to

improve ocular bioavailability following topical application. In this study, NFX-loaded polymeric nanoparticles for ocular application were successfully prepared with a spherical morphology using the spray drying method. DSC analysis confirmed the amorphous nature of the nanoparticles. Characterization by FT-IR and ^{1}H-NMR demonstrated that NFX remained stable throughout the formulation processes.

The nanoparticles exhibited a particle size of 383.43 ± 8.01 nm, a PDI of 0.135 ± 0.01, and a positive zeta potential of +34.97 ± 0.22 mV. Crucially, the optimized nanoparticles exhibited particle sizes well below the 10 µm threshold, ensuring their suitability for ocular administration by minimizing irritation and facilitating effective permeation. Additionally, the drug loading study indicated that NFX was incorporated into the polymers in sufficient amounts. The NEP formulations exhibited increased EE% and DL% compared to the NE formulations. The inclusion of PCL in the formulation had a positive effect on the particle characteristics. Among the formulations studied, NEP3 formulation distinguished itself by demonstrating superior physical stability, higher NFX loading and prolonged release properties. The prepared nanoparticles were successfully dispersed colloidally in NFX artificial tears, despite the drug's very low water solubility. The amorphous structure of the polymers contributed to improved solubility. Furthermore, *in vitro* release studies demonstrated that bioavailability could be enhanced by formulating nanoparticles suitable for ocular application with sustained release extending up to 48 hours. The release of NFX from the nanoparticles was found to be optimally modeled by the Korsmeyer-Peppas kinetics, suggesting a mechanism governed by both diffusion and polymer properties. Moreover, the initial drug release from the nanoparticles guarantees immediate therapeutic action, as the local drug concentration rapidly exceeds the required MIC.

Cytotoxicity assays conducted on ARPE-19 cells confirmed that the IC_{50} values of the nanoparticle formulations significantly exceeded their MICs. For instance, while the MIC of the optimal NEP3 formulation was 0.04 µg.mL^{-1}, its IC_{50} values ranged between 366.5 and 443.6 µg.mL^{-1}, thereby validating a remarkably broad therapeutic safety margin for topical ocular application.

Antimicrobial activity tests, particularly the disc diffusion method, showed that Gram-positive bacteria (*B. subtilis* and *S. aureus*) showed higher susceptibility compared to their Gram-negative counterparts. Notably, formulations NE3 and NEP3 displayed superior

efficacy, with inhibition values increasing in a dose-dependent manner. The coherence between the disc diffusion and MIC test results strongly validates the potential of the NFX-loaded nanoparticles as an effective system for treating ocular infections. In conclusion, NFX-loaded nanoparticles are anticipated to be a promising and effective alternative for the clinical management of ocular bacterial infections which will be with revealed more clearly with upcoming *in vivo* studies.

Acknowledgement

The authors would like to thank to Anadolu University-BİBAM for SEM and ^{1}H-NMR analyses, to Anadolu University-MERLAB for FT-IR analyses and to Assist. Prof. Dr. Sibel Çetinel from Sabancı University Nanotechnology Research and Application Center (SUNUM) for providing the ARPE-19 cell lines.

Author contribution

EB: Conceptualization, supervision, study design and manuscript revision. IO: Data collection, analyses and writing the manuscript. KA: Data collection and analyses. CKO: Cytotoxicity analyses. BŞ: Cytotoxicity analyses. PS: Antimicrobial activity studies.

Funding

This study was supported by Anadolu University Scientific Research Projects Coordination Unit (Project Number: 3677).

Data availability

The datasets generated during and/or analysed during the current study are available from the corresponding author on reasonable request.

Declarations

Competing interest

The authors declare that they have no known competing financial interests or personal relationships that could have appeared to influence the work reported in this paper.

Ethics statement

Not applicable.

Consent to Participate

Not applicable.

Consent to Publish declarations

Not applicable.

References

1. Ubani U. Common Bacterial Isolates From Infected Eyes. Journal of the Nigerian Optometric Association. 2009;15:40–7. https://doi.org/10.4314/jnoa.v15i1.55610

2. Høvding G. Acute bacterial conjunctivitis. Acta Ophthalmol John. 2008;86:5–17. https://doi.org/10.1111/j.1600-0420.2007.01006.x

3. Epling J. Bacterial conjunctivitis. BMJ Clin Evid 2012. 2012;0704. https://pmc.ncbi.nlm.nih.gov/articles/PMC3635545/

4. Bertino JS. Impact of antibiotic resistance in the management of ocular infections: The role of current and future antibiotics. Clinical Ophthalmology. 2009; 3:507–21. https://doi.org/10.2147/opth.s5778

5. Snyder RW, Glasser DB. Antibiotic therapy for ocular infection. Western Journal of Medicine. 1994;161:579. https://pmc.ncbi.nlm.nih.gov/articles/PMC1022739/

6. Sood D, Kumar N, Singh A, Sakharkar MK, Tomar V, Chandra R. Antibacterial and Pharmacological Evaluation of Fluoroquinolones: A Chemoinformatics Approach. Genomics Inform. 2018;16:44. https://doi.org/10.5808/GI.2018.16.3.44

7. Barry AL, Jones RN, Thornsberry C, Ayers LW, Gerlach EH, Sommers HM. Antibacterial activities of ciprofloxacin, norfloxacin, oxolinic acid, cinoxacin, and nalidixic acid. Antimicrob Agents Chemother. 1984;25:633–7. https://doi.org/10.1128/aac.25.5.633

8. Chierentin L, Regina H, Salgado N, Erida H, Salgado RN. Review of Properties and Analytical Methods for the Determination of Norfloxacin. Crit Rev Anal Chem. 2016;46:22–39. https://doi.org/10.1080/10408347.2014.941456

9. Naumann P, Dopp C. Fluoroquinolones--antibacterial activity, pharmacokinetics and indications for a new group of chemotherapeutic drugs. Internist (Berl). 1989;30:20–31. https://europepmc.org/article/med/2646237

10. Giardini F, Grandi G, De Sanctis U, Eandi C, Machetta F, Pollino C, et al. *In vitro* susceptibility to different topical ophthalmic antibiotics of bacterial isolates from patients with conjunctivitis. Ocul Immunol Inflamm. 2011;19:419–21. https://doi.org/10.3109/09273948.2011.624289

11. Swanson BN, Boppana VK, Vlasses PH, Rotmensch HH, Ferguson RK. Norfloxacin disposition after sequentially increasing oral doses. Antimicrob Agents Chemother. 1983 ;23:284–8. https://doi.org/10.1128/aac.23.2.284

12. Polat HK, Pehlivan SB, Çalış S. Bakteriyel Keratit Tedavisinde Yeni İlaç Taşıyıcı Sistemlerin Uygulanması. Turkiye Klinikleri Journal of Ophthalmology. 2018;27:289–301. https://doi.org/10.5336/ophthal.2017-57139

13. Morrison PWJ, Khutoryanskiy V V. Advances in Ophthalmic Drug Delivery. Ther Deliv. 2014;5:1297–315. https://doi.org/10.4155/tde.14.75

14. Mofidfar M, Abdi B, Ahadian S, Mostafavi E, Desai TA, Abbasi F, et al. Drug delivery to the anterior segment of the eye: A review of current and future treatment strategies. Int J Pharm. 2021;607:120924. https://doi.org/10.1016/j.ijpharm.2021.120924

15. Lanier OL, Manfre MG, Bailey C, Liu Z, Sparks Z, Kulkarni S, et al. Review of Approaches for Increasing Ophthalmic Bioavailability for Eye Drop Formulations. AAPS PharmSciTech. 2021;22:1–16. https://doi.org/10.1208/s12249-021-01977-0

16. Bairagi RD, Reon RR, Hasan MM, Sarker S, Debnath D, Rahman MT, et al. Ocular drug delivery systems based on nanotechnology: a comprehensive review for the treatment of eye diseases. Discover Nano. 2025;20:1–43. https://doi.org/10.1186/s11671-025-04234-6

17. Singhvi G, Banerjee S, Khosa A. Lyotropic liquid crystal nanoparticles: A novel improved lipidic drug delivery system. Organic Materials as Smart Nanocarriers for Drug Delivery. 2018;471–517. https://doi.org/10.1016/B978-0-12-813663-8.00011-7

18. Bachu RD, Chowdhury P, Al-Saedi ZHF, Karla PK, Boddu SHS. Ocular Drug Delivery Barriers—Role of Nanocarriers in the Treatment of Anterior Segment Ocular Diseases. Pharmaceutics. 2018;10:28. https://doi.org/10.3390/pharmaceutics10010028

19. Cal K, Sollohub K. Spray Drying Technique. I: Hardware and Process Parameters. J Pharm Sci. 2010;99:575–86. https://doi.org/10.1002/jps.21886

20. Bedor DCG, Gonçalves TM, Bastos LL, De Sousa CEM, De Abreu LRP, Oliveira EDJ, et al. Development and validation of a new method for the quantification of norfloxacin by HPLC-UV and its application to a comparative pharmacokinetic study in human volunteers. Revista Brasileira de Ciências Farmacêuticas. 2007;43:231–8. https://doi.org/10.1590/S1516-93322007000200009

21. Başaran E. Ocular Application of Dirithromycin Incorporated Polymeric Nanoparticles: an *In Vitro* Evaluation. Turk J Pharm Sci. 2017;14:191. https://dx.doi.org/10.4274/tjps.69855

22. Bruschi M. Strategies to modify the drug release from pharmaceutical systems. [E-book]. 2015. Accessed: Jul. 22, 2025. https://books.google.com.tr/books?id=K8cmEQAAQBAJ

23. Lin H, Yue Y, Maidana DE, Bouzika P, Atik A, Matsumoto H, et al. Drug Delivery Nanoparticles: Toxicity Comparison in Retinal Pigment Epithelium and Retinal Vascular

Endothelial Cells. Semin Ophthalmol. 2016;31:1–9. https://doi.org/10.3109/08820538.2015.1114865

24. Özer S, Şenel B, Yazan Y. Preparation and *in vitro* evaluation of in situ gelling system containing lithium carbonate for parenteral administration. Polymer Bulletin. 2020;77:599–622. https://doi.org/10.1007/s00289-019-02764-5

25. Bauer AW, Kirby WM, Sherris JC, Turck M. Antibiotic Susceptibility Testing by a Standardized Single Disk Method. Am J Clin Pathol. 1966;45:493–6. https://doi.org/10.1093/ajcp/45.4_ts.493

26. CLSI. M02 | Performance Standards for Antimicrobial Disk Susceptibility Tests. [Standard]. Accessed: Oct. 26, 2025. https://clsi.org/shop/standards/m02/

27. CLSI. M07 | Methods for Dilution Antimicrobial Susceptibility Tests for Bacteria That Grow Aerobically. [Standard]. Accessed: Oct. 26, 2025. https://clsi.org/shop/standards/m07/

28. Gebreel RM, Edris NA, Elmofty HM, Tadros MI, El-Nabarawi MA, Hassan DH. Development and characterization of PLGA nanoparticle-laden hydrogels for sustained ocular delivery of norfloxacin in the treatment of pseudomonas keratitis: An experimental study. Drug Des Devel Ther. 2021;15:399–418. https://doi.org/10.2147/DDDT.S293127

29. Bahari LAS, Hamishehkar H. The Impact of Variables on Particle Size of Solid Lipid Nanoparticles and Nanostructured Lipid Carriers; A Comparative Literature Review. Adv Pharm Bull. 2016;6:143. https://doi.org/10.15171/apb.2016.021

30. Ozturk A, Yenilmez E, Arslan R, Şenel B, Yazan Y. Dexketoprofen Trometamol-Loaded Kollidon (R) SR and Eudragit (R) RS 100 Polymeric Nanoparticles: Formulation and *In Vitro-In Vivo* Evaluation. Latin American Journal of Pharmacy. 2017;36. http://www.latamjpharm.org/resumenes/36/11/LAJOP_36_11_1_4.pdf

31. Wu R, Huang Q, Zhou Z, Chen Y, Hu H, Wang F, et al. Nanoparticulate ophthalmic drug delivery of norfloxacin to prevent ocular infection after cataract surgery: Evaluation in animal model. Materials Express. 2021;11:1402–11. https://doi.org/10.1166/mex.2021.2040

32. Kaur IP, Kanwar M. Ocular Preparations: The Formulation Approach. Drug Dev Ind Pharm. 2002;28:473–93. https://doi.org/10.1081/DDC-120003445

33. Ban J, Zhang Y, Huang X, Deng G, Hou D, Chen Y, et al. Corneal permeation properties of a charged lipid nanoparticle carrier containing dexamethasone. Int J Nanomedicine. 2017;12:1329–39. https://doi.org/10.2147/IJN.S126199

34. Başaran E, Yenilmez E, Berkman MS, Büyükköroğlu G, Yazan Y. Chitosan nanoparticles for ocular delivery of cyclosporine A. J Microencapsul. 2014;31:49–57. https://doi.org/10.3109/02652048.2013.805839

35. Almeida H, Amaral MH, Lobão P, Silva AC, Lobo JMS. Applications of polymeric and lipid nanoparticles in ophthalmic pharmaceutical formulations: present and future considerations. J Pharm Pharm Sci. 2014;17:278–93. https://doi.org/10.18433/j3dp43

36. Freitas C, Müller RH. Effect of light and temperature on zeta potential and physical stability in solid lipid nanoparticle (SLN^{TM}) dispersions. Int J Pharm.1998;168:221–9. https://doi.org/10.1016/S0378-5173(98)00092-1

37. Bhattacharjee S. In relation to the following article "DLS and zeta potential — What they are and what they are not?" Journal of Controlled Release, 2016, 235, 337–351. Journal of Controlled Release. 2016;238:311–2. https://doi.org/10.1016/j.jconrel.2016.06.017

38. Radomska-Soukharev A. Stability of lipid excipients in solid lipid nanoparticles. Adv Drug Deliv Rev. 2007;59:411–8. https://doi.org/10.1016/j.addr.2007.04.004

39. Tsai CH, Wang PY, Lin IC, Huang H, Liu GS, Tseng CL. Ocular Drug Delivery: Role of Degradable Polymeric Nanocarriers for Ophthalmic Application. International Journal of Molecular Sciences. 2018;19:2830. https://doi.org/10.3390/ijms19092830

40. Yenilmez E. Desloratadine-Eudragit® RS100 Nanoparticles: Formulation and Characterization. Turk J Pharm Sci. 2017;14:148. https://doi.org/10.4274/tjps.52523

41. Borges O, Borchard G, Verhoef JC, De Sousa A, Junginger HE. Preparation of coated nanoparticles for a new mucosal vaccine delivery system. Int J Pharm. 2005;299:155–66. https://doi.org/10.1016/j.ijpharm.2005.04.037

42. Ribeiro AJ, Silva C, Ferreira D, Veiga F. Chitosan-reinforced alginate microspheres obtained through the emulsification/internal gelation technique. European Journal of Pharmaceutical Sciences. 2005;25:31–40. https://doi.org/10.1016/j.ejps.2005.01.016

43. Khan MA, Khan S, Kazi M, Alshehri SM, Shahid M, Khan SU, et al. Norfloxacin Loaded Lipid Polymer Hybrid Nanoparticles for Oral Administration: Fabrication, Characterization, In Silico Modelling and Toxicity Evaluation. Pharmaceutics. 2021;13:1632. https://doi.org/10.3390/pharmaceutics13101632

44. Dhevaraj J, Vembu S, Pazhamalai S, Gopalakrishnan M. "Design and Synthesis of Some Cyclic Carbohydrates with Norfloxacin as Surface moiety. A Study of Sustained Relax of Drugs". Oriental Journal of Chemistry. 2019;35:577–90. https://doi.org/10.13005/ojc/350211

45. Al-Heibshy FNS, Başaran E, Arslan R, Öztürk N, Erol K, Demirel M. Physicochemical characterization and pharmacokinetic evaluation of rosuvastatin calcium incorporated solid lipid nanoparticles. Int J Pharm. 2020;578:119106. https://doi.org/10.1016/j.ijpharm.2020.119106

46. Seremeta KP, Chiappetta DA, Sosnik A. Poly(ε-caprolactone), Eudragit® RS 100 and poly(ε-caprolactone)/Eudragit® RS 100 blend submicron particles for the sustained release of the antiretroviral efavirenz. Colloids Surf B Biointerfaces. 2013;102:441–9. https://doi.org/10.1016/j.colsurfb.2012.06.038

47. Badri W, Miladi K, Robin S, Viennet C, Nazari QA, Agusti G, et al. Polycaprolactone Based Nanoparticles Loaded with Indomethacin for Anti-Inflammatory Therapy: From Preparation to *Ex Vivo* Study. Pharm Res. 2017;34:1773–83. https://doi.org/10.1007/s11095-017-2166-7

48. ICH. ICH Q2(R1) | Validation of Analytical Procedures: Text and Methodology Q2(R1). [Guideline]. 2005. https://database.ich.org/sites/default/files/Q2%28R1%29%20Guideline.pdf

49. Thagele R, Mishra A, Sci AP-IJPL, 2011 undefined. Formulation and characterization of clarithromycin based nanoparticulate drug delivery system. Int J Pharm Life Sci. 2011; 2(1): 510–515. https://www.researchgate.net/publication/301888112_Formulation_and_Characterization_of_Clarithromycin_Nanoparticulate_Drug_Delivery_System

50. Mudgil M, Pawar PK. Preparation and *In Vitro/Ex Vivo* Evaluation of Moxifloxacin-Loaded PLGA Nanosuspensions for Ophthalmic Application. Sci Pharm. 2013;81:591. https://doi.org/10.3797/scipharm.1204-16

51. Zhang Y, Huo M, Zhou J, Zou A, Li W, Yao C, et al. DDSolver: An Add-In Program for Modeling and Comparison of Drug Dissolution Profiles. The AAPS Journal. 2010;12:263–71. https://doi.org/10.1208/S12248-010-9185-1

52. Bohrey S, Chourasiya V, Pandey A. Polymeric nanoparticles containing diazepam: Preparation, optimization, characterization, in-vitro drug release and release kinetic study. Nano Converg. 2016;3:1–7. https://doi.org/10.1186/s40580-016-0061-2

53. Costa P, Sousa Lobo JM. Modeling and comparison of dissolution profiles. European Journal of Pharmaceutical Sciences. 2001;13:123–33. https://doi.org/10.1016/S0928-0987(01)00095-1

54. Mittal B. How to Develop Robust Solid Oral Dosage Forms: From Conception to Post-Approval. [Book/Monograph]. 2016: 1–168. https://doi.org/10.1016/c2015-0-01916-5

55. Dash S, Murthy PN, Nath L, Chowdhury P. Kinetic modeling on drug release from controlled drug delivery systems. Acta Pol Pharm. 2010;67(3):217-23. https://pubmed.ncbi.nlm.nih.gov/20524422/

56. Trapani A, Laquintana V, Denora N, Lopedota A, Cutrignelli A, Franco M, et al. Eudragit RS 100 microparticles containing 2-hydroxypropyl-β-cyclodextrin and glutathione: Physicochemical characterization, drug release and transport studies. European Journal of Pharmaceutical Sciences. 2007;30:64–74. https://doi.org/10.1016/j.ejps.2006.10.003

57. Sinha VR, Bansal K, Kaushik R, Kumria R, Trehan A. Poly-ϵ-caprolactone microspheres and nanospheres: an overview. Int J Pharm. 2004;278:1–23. https://doi.org/10.1016/j.ijpharm.2004.01.044

58. Talaei S, Mahboobian MM, Mohammadi M. Investigating the ocular toxicity potential and therapeutic efficiency of in situ gel nanoemulsion formulations of brinzolamide. Toxicol Res. 2020;9:578–87. https://doi.org/10.1093/toxres/tfaa066

59. Ansari M, Kulkarni YA, Singh K. Ocular polymeric nanomicelles for the posterior eye segment in the management of retinoblastoma: formulation, optimization, *in vitro* and

ex vivo evaluations. Pharm Dev Technol. 2025;30:246–58. https://doi.org/10.1080/10837450.2025.2469321

60. Moe B, Berezowski KL, Huang DY, Dey I, Xie L, Ling ZC, et al. A microelectric cell sensing technique for *in vitro* assessment of ocular irritation. Toxicology *in Vitro*. 2021;73:105124. https://doi.org/10.1016/j.tiv.2021.105124

61. Bhatt P, Narvekar P, Lalani R, Chougule MB, Pathak Y, Sutariya V. An *in vitro* Assessment of Thermo-Reversible Gel Formulation Containing Sunitinib Nanoparticles for Neovascular Age-Related Macular Degeneration. AAPS PharmSciTech. 2019;20:281. https://doi.org/10.1208/s12249-019-1474-0

62. Abriata JP, Turatti RC, Luiz MT, Raspantini GL, Tofani LB, do Amaral RLF, et al. Development, characterization and biological *in vitro* assays of paclitaxel-loaded PCL polymeric nanoparticles. Materials Science and Engineering: C. 2019;96:347–55. https://doi.org/10.1016/j.msec.2018.11.035

63. Bhattacharya S. Genotoxicity and *in vitro* investigation of Gefitinib-loaded polycaprolactone fabricated nanoparticles for anticancer activity against NCI-H460 cell lines. J Exp Nanosci. 2022;17:214–46. https://doi.org/10.1080/17458080.2022.2060501

64. Łukasiewicz S, Mikołajczyk A, Błasiak E, Fic E, Dziedzicka-Wasylewska M. Polycaprolactone Nanoparticles as Promising Candidates for Nanocarriers in Novel Nanomedicines. Pharmaceutics. 2021;13:191. https://doi.org/10.3390/pharmaceutics13020191

65. Fröhlich E. The role of surface charge in cellular uptake and cytotoxicity of medical nanoparticles. Int J Nanomedicine. 2012;7:5577–91. https://doi.org/10.2147/IJN.S36111

66. dos Santos RB, Funguetto-Ribeiro AC, Maciel TR, Fonseca DP, Favarin FR, Nogueira-Librelotto DR, et al. *In vivo* and *in vitro* per se effect evaluation of Polycaprolactone and Eudragit® RS100-based nanoparticles. Biomedicine & Pharmacotherapy. 2022;153:113410. https://doi.org/10.1016/j.biopha.2022.113410

67. Jesus S, Bernardi N, Da Silva J, Colaço M, Panaõ Costa J, Fonte P, et al. Unravelling the Immunotoxicity of Polycaprolactone Nanoparticles—Effects of Polymer Molecular Weight, Hydrolysis, and Blends. Chem Res Toxicol. 2020;33:2819–33. https://doi.org/10.1021/acs.chemrestox.0c00208

68. Fan TJ, Wu SX, Jiang GJ. Apoptotic effects of norfloxacin on corneal endothelial cells. Naunyn Schmiedebergs Arch Pharmacol. 2020;393:77–88. https://doi.org/10.1007/s00210-019-01711-5

69. Nikaido H. Molecular Basis of Bacterial Outer Membrane Permeability Revisited. Microbiology and Molecular Biology Reviews. 2003;67:593–656. https://doi.org/10.1128/mmbr.67.4.593-656.2003

70. Lister PD, Wolter DJ, Hanson ND. Antibacterial-Resistant Pseudomonas aeruginosa: Clinical Impact and Complex Regulation of Chromosomally Encoded Resistance Mechanisms. Clin Microbiol Rev. 2009;22:582–610. https://doi.org/10.1128/cmr.00040-09

71. Adepu S, Ramakrishna S, Costa-Pinto R, Oliveira AL. Controlled Drug Delivery Systems: Current Status and Future Directions. Molecules. 2021;26:5905. https://doi.org/10.3390/molecules26195905